Mon. Not. R. Astron. Soc. **000**, 000–000 (0000) Printed 31 March 2015 (MN LATEX style file v2.2)

On the interpretation of sub-giant branch morphologies of intermediate-age star clusters with extended main sequence turnoffs

Paul Goudfrooij,[1⋆] Léo Girardi,[2] Philip Rosenfield,[3] Alessandro Bressan,[4] Paola Marigo,[3] Matteo Correnti,[1] and Thomas H. Puzia[5]

[1] *Space Telescope Science Institute, 3700 San Martin Drive, Baltimore, MD 21218, U.S.A.*
[2] *Osservatorio Astronomico di Padova – INAF, Vicolo dell'Osservatorio 5, I-35122 Padova, Italy*
[3] *Dipartimento di Fisica e Astronomia Galileo Galilei, Università di Padova, Vicolo dell'Osservatorio 3, I-35122 Padova, Italy*
[4] *SISSA, via Bonomea 365, I-34136 Trieste, Italy*
[5] *Institute of Astrophysics, Pontificia Universidad Católica de Chile, Av. Vicuña Mackenna 4860, 7820436 Macul, Santiago, Chile*

Accepted 2015 March 25. Received 2015 March 10; in original form 2015 February 5

ABSTRACT

Recent high-quality photometry of many star clusters in the Magellanic Clouds with ages of 1 – 2 Gyr revealed main sequence turnoffs (MSTOs) that are significantly wider than can be accounted for by a simple stellar population (SSP). Such extended MSTOs (eMSTOs) are often interpreted in terms of an age spread of several 10^8 yr, challenging the traditional view of star clusters as being formed in a single star formation episode. Li et al. and Bastian & Niederhofer recently investigated the sub-giant branches (SGBs) of NGC 1651, NGC 1806, and NGC 1846, three star clusters in the Large Magellanic Cloud (LMC) that exhibit an eMSTO. They argued that the SGB of these star clusters can be explained only by a SSP. We study these and two other similar star clusters in the LMC, using extensive simulations of SSPs including unresolved binaries. We find that the shapes of the cross-SGB profiles of all star clusters in our sample are in fact consistent with their cross-MSTO profiles when the latter are interpreted as age distributions. Conversely, SGB morphologies of star clusters with eMSTOs are found to be inconsistent with those of simulated SSPs. Finally, we create PARSEC isochrones from tracks featuring a grid of convective overshoot levels and a very fine grid of stellar masses. A comparison of the observed photometry with these isochrones shows that the morphology of the red clump (RC) of such star clusters is also consistent with that implied by their MSTO in the age spread scenario. We conclude that the SGB and RC morphologies of star clusters featuring eMSTOs are consistent with the scenario in which the eMSTOs are caused by a distribution of stellar ages.

Key words: galaxies: Magellanic Clouds, star clusters; globular clusters: general; stars: Hertzsprung-Russell and colour-magnitude diagrams

1 INTRODUCTION

Until recently, globular clusters (GCs) were thought to be simple stellar populations (hereafter SSPs), consisting of thousands to millions of coeval stars with the same chemical composition. In the past decade, however, a consensus has emerged that GCs typically harbor multiple stellar populations featuring several unexpected characteristics (e.g., Bedin et al. 2004; Piotto et al. 2007; Gratton et al. 2012, and references therein). Multiple sequences in several major features of colour-magnitude diagrams (CMDs) are now commonplace in massive Galactic star clusters, e.g, in their main sequence (MS), sub-giant branch (SGB), and red giant branch (RGB). These multiple sequences are especially evident in *Hubble Space Telescope (HST)* photometry using colours involving passbands that cover molecular features of OH, NH, and CN in the near-ultraviolet part of the electromagnetic spectrum (see, e.g., Piotto et al. 2012; Bellini et al. 2013; Milone et al. 2012, 2013, 2015; Dotter et al. 2015).

Meanwhile, recent spectroscopic surveys established that light elements such as N, O, and Na show large star-to-star abundance variations (often dubbed "Na-O anticorrelations") within virtually all Galactic GCs studied to date in sufficient detail (Carretta et al. 2010, and references therein). The chemical processes involved in causing the light-element abundance variations have largely been identified as proton capture reactions at high temperature ($T \gtrsim 2 \times 10^7$ K), such as the CNO and NeNa cycles. Currently, the leading candidates for polluting sources ("polluters") are stars in which such reactions occur readily and which feature slow stellar winds

⋆ E-mail: goudfroo@stsci.edu

so that their ejecta are relatively easy to retain within the potential well of massive clusters: (1) intermediate-mass asymptotic giant branch (AGB) and super-AGB stars ($4 \lesssim \mathcal{M}/M_{\odot} \lesssim 10$; e.g., D'Antona & Ventura 2007), (2) rapidly rotating massive stars (often referred to as "FRMS"; Decressin et al. 2007) and (3) massive binary stars (de Mink et al. 2009).

In the two currently favored formation scenarios, these chemical anticorrelations are due to stars having either formed from or polluted by gas that is a mixture of pristine material and material shed by such polluters. In the "extended star formation" scenario (see, e.g., D'Ercole et al. 2008; Conroy & Spergel 2011; Vancarce & Catelan 2011), the abundance variations are caused by a second generation of stars that formed out of gas clouds that were polluted by winds of first-generation stars to varying extents, during a period spanning up to a few hundreds of Myr, depending on the nature of the polluters and the depth of the potential well. The alternative "early disc accretion" scenario (Bastian et al. 2013) does *not* involve extended star formation: the polluted gas is instead produced by FRMS and massive binary stars, and accreted by low-mass pre-main-sequence stars during the first ≈ 20 Myr after the formation of the star cluster.

In the context of the nature of Na-O anticorrelations in Galactic GCs, the recent discovery of extended main sequence turn-offs (hereafter eMSTOs) in intermediate-age (1 – 2 Gyr old) star clusters in the Magellanic Clouds (Mackey & Broby Nielsen 2007; Mackey et al. 2008; Glatt et al. 2008; Milone et al. 2009; Goudfrooij et al. 2009, 2011a,b) has generated much interest. Several investigations suggested that the eMSTOs are due to the presence of multiple stellar populations spanning an age interval of several 10^8 yr within these clusters (see also Rubele, Kerber, & Girardi 2010; Rubele et al. 2011; Keller, Mackey, & Da Costa 2011, 2012; Girardi et al. 2013a; Correnti et al. 2014; Goudfrooij et al. 2014). The leading alternative theory for the cause of the eMSTO phenomenon is that it is due to spreads in rotation velocity among turnoff stars (hereafter the "stellar rotation" scenario: Bastian & de Mink 2009; Li et al. 2012; Yang et al. 2013; Li, de Grijs, & Deng 2014, but see Girardi et al. 2011).

Due to the important implications of the answer to the question whether or not eMSTOs in intermediate-age clusters are due to a significant range in stellar ages, the issue is being studied from a variety of angles. Recent investigations looked for evidence of extended star formation (or a significant lack thereof) in young massive star clusters in the Large Magellanic Cloud (LMC), with seemingly conflicting results (see Bastian & Silva-Villa 2013 versus Correnti et al. 2015). Others studied relations between properties of eMSTOs and dynamical properties of the clusters, finding a correlation between eMSTO width and cluster escape velocity which seems to be understood most straightforwardly in terms of the extended star formation scenario (Goudfrooij et al. 2014, hereafter G+14). However, results with the opposite conclusion were recently reported by Li et al. (2014, hereafter L+14) and Bastian & Niederhofer (2015, hereafter BN15). L+14 studied the SGB morphology of NGC 1651, an eMSTO cluster of age $\simeq 2$ Gyr, and concluded that it can be explained only by a single-age stellar population. Showing results of new calculations of stellar tracks in the MSTO-SGB region of the CMD with vs. without stellar rotation, L+14 argued that eMSTOs in intermediate-age clusters are most likely caused by a range of stellar rotation velocities within such clusters. BN15 performed a similar study of the SGB morphologies in NGC 1806 and NGC 1846, two other eMSTO clusters, again concluding that age spreads are unlikely to be the cause of the eMSTO phenomenon.

In the current paper, we investigate the claims of L+14 and BN15 by means of an independent study of the SGB properties of five intermediate-age star clusters in the LMC (including the clusters studied by L+14 and BN15). After a brief description of the data and SSP models used in this paper in Sect. 2, we discuss properties of cross-SGB magnitude distributions for these star clusters and highlight differences with the methodologies used by L+14 and BN15 in Sect. 3. Sect. 4 reviews the relevance of convective overshoot to the morphology of the CMD of intermediate-age clusters, and discusses our cross-SGB distributions when compared with a set of isochrones in which the implementation of the dependence of convective overshoot on stellar mass is different from that used in the isochrones used by L+14 and BN15. Sect. 4 also includes an investigation of the claim by BN15 that the morphologies of the red clumps in these star clusters are inconsistent with the age spread scenario. Our conclusions and their implications are summarized in Sect. 5.

2 DATA AND MODELS

We use the *HST* photometry of intermediate-age star clusters in the LMC that was described in detail in Goudfrooij et al. (2011a, hereafter G+11a), G+14, and Correnti et al. (2014). Briefly, the data from G+11a used here involves multi-exposure photometry taken with the Wide Field Camera (WFC) of the Advanced Camera for Surveys (ACS) using the F435W and F814W filters (*HST* program 10595, PI: P. Goudfrooij). The data from G+14 used here involves similar photometry, now taken with the Wide Field Camera #3 (WFC3) using the F475W and F814W filters (*HST* program 12257, PI: L. Girardi), while the data from Correnti et al. (2014) used here involves ACS/WFC photometry using the F555W and F814W filters with one exposure per filter (*HST* "snapshot" program 9891, PI: G. Gilmore).

From this sample we first select the star clusters in the LMC for which the eMSTO feature is clearly established. Specifically, we select star clusters for which G+14 measured full-width at half maximum (FWHM) values of their MSTO cross-cut of at least 350 Myr when expressed as an age range (i.e., their "pseudo-age distributions"). Since we are interested in measuring the SGB morphologies of such clusters, we subselect clusters for which their CMD includes at least 35 stars in the SGB region[1]. This selection procedure yields the three massive clusters NGC 1783, NGC 1806, and NGC 1846. To this sample we add NGC 1651 (which also features an eMSTO), the cluster for which Li et al. (2014) claimed that its SGB morphology can be explained only by a single-age stellar population. Finally, we add IC 2146, a cluster whose mass and age are very similar to those of NGC 1651 although it does *not* show evidence for an eMSTO. We find that the SGB properties of IC 2146 reveal information that is relevant to the question whether or not (and, if so, how) SGB morphologies of eMSTO clusters can be used to rule out extended star formation periods. Relevant properties of the star clusters in our sample are listed in Table 1.

To avoid issues related to the presence of a significant number of LMC field stars in relevant parts of the CMDs, we only consider stars within the core radius of the clusters. The only exception to this is the case of NGC 1651 for which the combination of cluster mass and core radius would yield too few stars in the SGB region

[1] We found that clusters with fewer than 30 – 35 SGB stars showed significant stochastic fluctuations in their cross-SGB magnitude distributions (see Sect. 3).

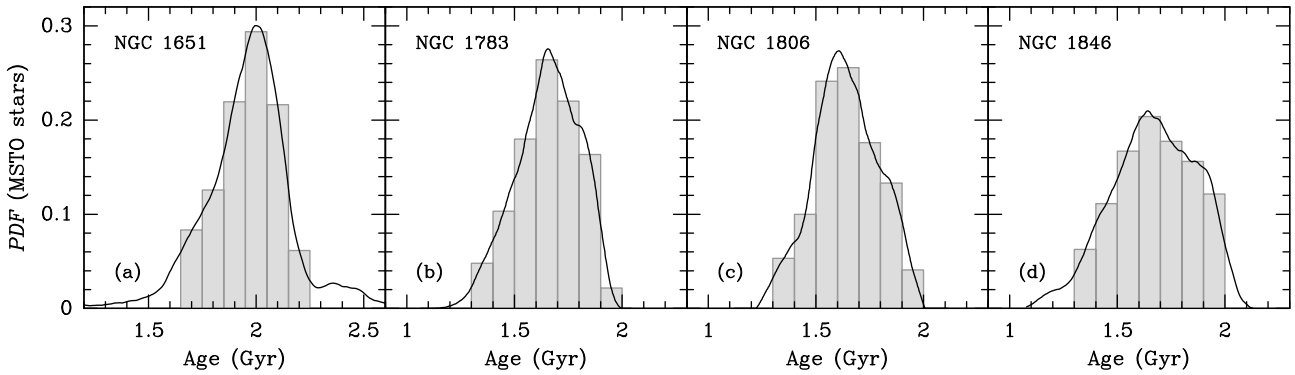

Figure 1. Illustration of the assignment of relative masses to individual SSP ages (i.e., isochrones) for the "multi-SSP" simulations of the 4 star clusters in our sample that feature eMSTOs (see Sect. 3.1). *Panel (a)*: The black solid line represents the pseudo-age distribution of NGC 1651 taken from G+14, expressed as probability density function (PDF). The histogram in light grey shows the relative weights of the different age bins used during the simulations. *Panel (b)*: Same as Panel (a), but now for NGC 1783, using its pseudo-age distribution taken from G+11a, using ages from the M+08 isochrones. *Panel (c)*: Same as Panel (b), but now for NGC 1806. *Panel (d)*: Same as Panel (b), but now for NGC 1846, using its pseudo-age distribution taken from Goudfrooij et al. (2009).

Table 1. Properties of star clusters in our sample.

Name	$\log \mathcal{M}_{\rm cl}$	r_c	$r_{\rm eff}$	Ref.	Age	Ref.
(1)	(2)	(3)	(4)	(5)	(6)	(7)
NGC 1651	4.91 ± 0.06	4.57 ± 0.36	12.82 ± 2.01	1	2.00	1
NGC 1783	5.42 ± 0.11	10.50 ± 0.49	11.40 ± 2.24	1	1.70	2
NGC 1806	5.10 ± 0.06	5.91 ± 0.27	9.04 ± 1.24	1	1.65	2
NGC 1846	5.24 ± 0.09	8.02 ± 0.49	8.82 ± 0.68	1	1.65	3
IC 2146	4.49 ± 0.07	8.89 ± 1.36	12.53 ± 1.92	4	1.90	4

Notes. Columns: (1) Name of star cluster. (2) Logarithm of cluster mass in $M_\odot$. (3) Core radius in pc. (4) Effective radius in pc. (5) Reference for cluster mass and radii (1 = G+14, 2 = G+11a, 3 = Goudfrooij et al. 2009, 4 = Correnti et al. 2014). (6) Age in Gyr used for the "single-SSP" simulations in Sect. 3. (7) Reference for age data.

to produce statistically robust results. Hence we use all stars within the effective radius for NGC 1651. The influence of field stars in the SGB region is negligible in all cases, as can be appreciated from the various CMD plots (panels (a) in Figs. 2 and 4 – 7).

We adopt the isochrones of Marigo et al. (2008, hereafter M+08) for much of our analysis in this paper, since these isochrones were also used by G+11a, G+14, L+14, Correnti et al. (2014), and BN15. For each cluster, we adopt the values for Z (always 0.008), distance $(m-M)_0$, best-fitting age, and foreground reddening (A_V) found by G+11a, G+14, and Correnti et al. (2014). The population properties of these clusters were determined from the brightnesses and colors of the MSTO and the RGB bump, and the slope of the RGB. The SGB morphology was not involved in the determination of cluster ages.

3 SGB MORPHOLOGIES

3.1 Method

To test whether the SGB morphologies of the clusters in this paper are best described by a single-age SSP or by a distribution of ages similar to those indicated by their MSTO morphologies (i.e., the pseudo-age distributions shown in G+11a and G+14), we create cross-SGB magnitude distributions (hereafter called "cross-SGB profiles") of the observations and compare them with such profiles derived from a set of Monte Carlo simulations of SSPs (including unresolved binary stars) as described below.

Candidate SGB stars are selected by means of a parallelogram in the CMD, illustrated in panels (a) – (c) of Fig. 2 by black dashed lines. The blue edge of the parallelogram is placed at a colour that is clearly redder than the MSTO feature, while the red edge of the parallelogram is placed at the colour reached by the SGB stars with the minimum luminosity in the relevant isochrones. The placement of the top and bottom of the parallelogram is guided by the distribution of stars in the various SSP simulations, making sure all artificial SGB stars are captured (including unresolved binaries) and verifying that the cluster's SGB stars are captured as well. Cross-SGB profiles are then created by measuring every star's magnitude offset from the isochrone with the best-fitting (mean) age as established in G+11a, G+14, and Correnti et al. (2014) at the colour of the star in question, using linear interpolation in colour space.

SSP simulations are conducted by populating isochrones with stars randomly drawn from a Salpeter (1955) IMF between the minimum and maximum stellar masses in the isochrone. We add unresolved binary companions to a fraction of the stars using the binary fractions found by G+11a, G+14, and Correnti et al. (2014), in conjunction with a flat primary-to-secondary mass ratio distribution. Finally, we add random photometric errors whose dependence on the location in the CMD was derived from the artificial star tests described by G+11a, G+14, and Correnti et al. (2014).

We perform two distinct sets of SSP simulations for each cluster: (1) a set of "single SSP" simulations, using the isochrone with the best-fitting (mean) age; (2) a set of "multi-SSP" (or "composite SSP") simulations. These use the isochrones whose ages encompass the range of ages indicated by the clusters' pseudo-age distributions that were derived from MSTO crosscut profiles by G+11a and G+14. We employ an age resolution of 0.1 Gyr. For each age, the relative number of stars used in the simulation is set by the median amplitude of the pseudo-age distribution for that age bin, in probability density units (this procedure is illustrated in Figure 1)[2]. The level to which such "multi-SSP" simulations approximate the relevant CMD features of the star cluster in question is illustrated

[2] This procedure is somewhat different from that used by BN15, who fitted single gaussians to the clusters' binned MSTO crosscut profiles.

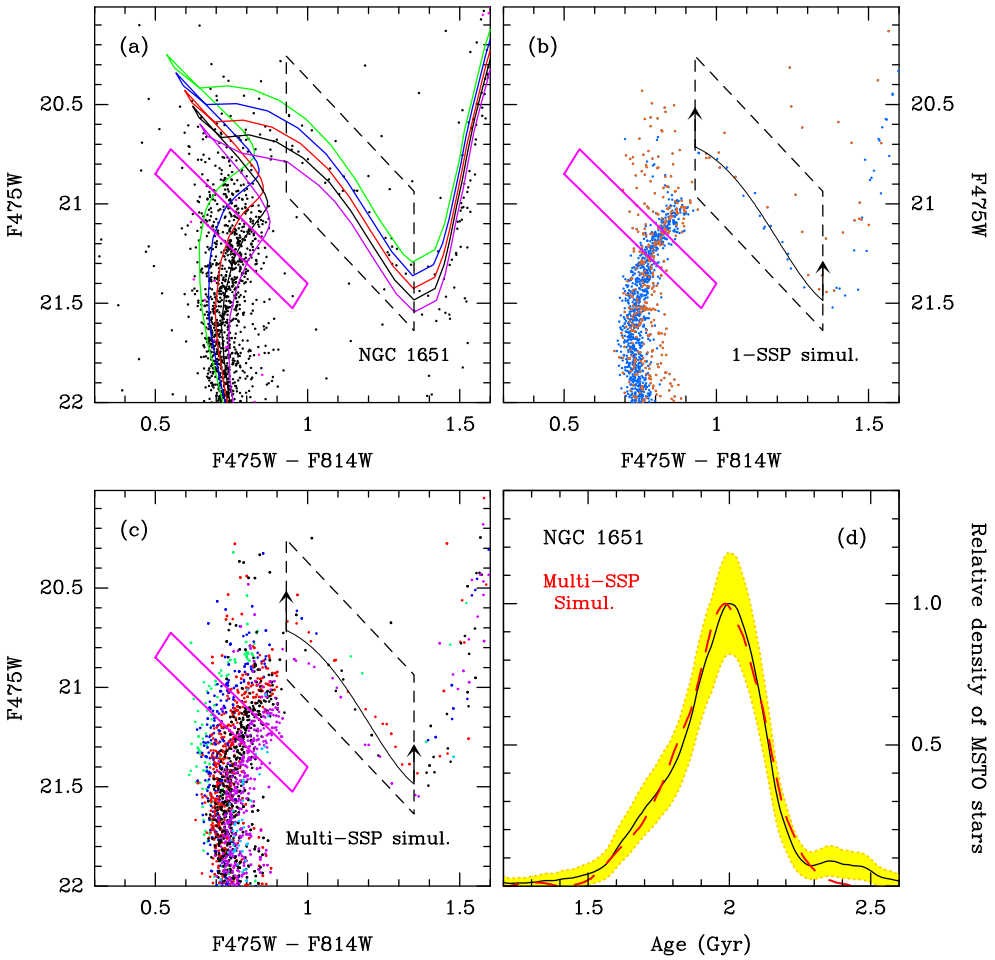

Figure 2. *Panel (a)*: the CMD of NGC 1651 in the MSTO-SGB region (taken from G+14) along with Marigo et al. (2008) isochrones for $Z = 0.008$ and ages 1.7, 1.8, 1.9, 2.0, and 2.1 Gyr. Black dots represent stars within the effective radius of NGC 1651. Red dots indicate stars in the outskirts of the *HST* image with a total area equal to that within the effective radius of NGC 1651. The SGB selection box is outlined by black dashed lines. For reference, the MSTO crosscut parallelogram used by G+14 to measure the pseudo-age distribution of NGC 1651 is shown in magenta. *Panel (b)*: CMD of a single-SSP simulation of NGC 1651 using the 2.0 Gyr isochrone (see Sect. 3.1). Single stars are shown as blue dots while unresolved binaries are shown as orange dots. The black solid line within the SGB selection box in panel (b) represents the SGB portion of the isochrone for the best-fitting (mean) age. The black arrows in panel (b) indicate the direction of the positive X axis in the cross-SGB profiles shown in Figures 3 – 7. *Panel (c)*: similar to panel (b) except that the dots now represent a "multi-SSP" simulation of NGC 1651, described in Sect. 3.1. Simulated stars with ages of 1.7, 1.8, 1.9, 2.0, 2.1, and 2.2 Gyr are shown in green, blue, red, black, purple, and cyan, respectively. *Panel (d)*: the black solid line represents the pseudo-age distribution of NGC 1651 as measured from the MSTO crosscut by G+14 (cf. Fig 1a), expressed as a normalised density function, while the yellow region indicates its 68% confidence interval. For comparison, the red dashed line represents the corresponding pseudo-age distribution of the "multi-SSP" simulation described in Sect. 3.1 for NGC 1651.

in Fig. 2 for the case of NGC 1651. In particular, panel (d) of Fig. 2 shows a comparison of the pseudo-age distribution of NGC 1651 as derived from its MSTO crosscut profile by G+14 (i.e., the curve shown also in Fig. 1a) with that of its "multi-SSP" set of simulations. The overall total number of stars in both sets of SSP simulations is normalised to the number of cluster stars on the CMD brighter than the 50% completeness limit. Finally, all individual simulations are repeated 20 times and their cross-SGB profiles are averaged together.

3.2 Results

3.2.1 NGC 1651

The resulting cross-SGB profiles for NGC 1651 are shown in Figure 3a. The profiles were derived as density functions, using the non-parametric Epanechnikov kernel (Silverman 1986). This minimizes biases that can arise if fixed bin widths are used.

The cross-SGB profile for the cluster itself (black solid line) shows some significant differences with that of the single-SSP simulation (blue line): the cross-SGB profile of the cluster is significantly wider than that of the single-SSP simulation, and there is an offset between the two profiles in that the cluster profile is centered on a F475W magnitude that is $\simeq 0.08$ mag brighter than that of the single-SSP simulation. The same offset is present between the profiles of the cluster and that of its "multi-SSP" simulation (see red solid line), while the *width* and shape of the latter are consistent with that of the cluster's profile (see dashed red line, which is offset by 0.08 mag from the solid red line in the positive X direction). *The similarity of the shapes of the cross-SGB profiles of the cluster and that of its multi-SSP simulation, along with the profile of the single-SSP simulation being significantly narrower, strongly suggests that the SGB morphology of NGC 1651 is better described by*

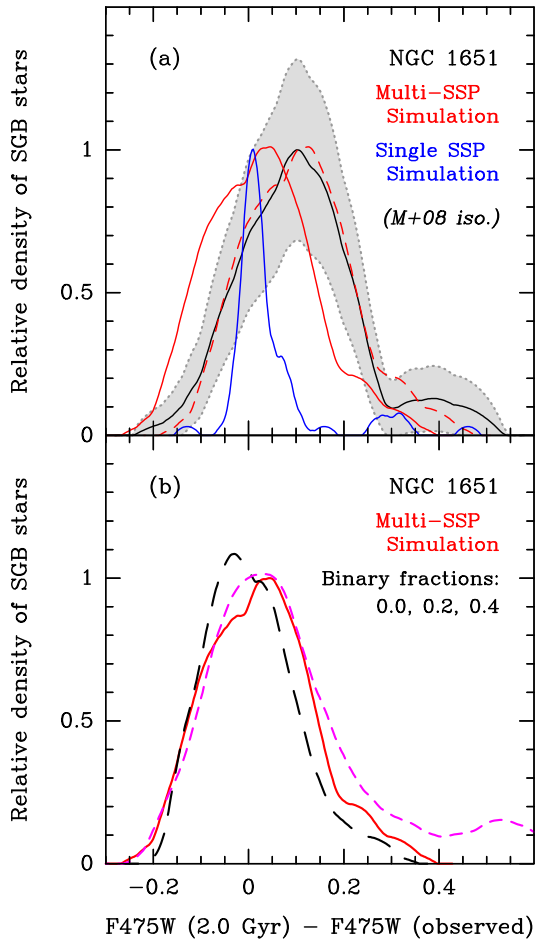

Figure 3. *Panel (a)*: The black solid line represents the cross-SGB profile for NGC 1651, while the light grey region indicates its 68% confidence interval. The red solid line represents the cross-SGB profile of the "multi-SSP" simulation described in Sect. 3.2.1. The red dashed line is the same after shifting it by 0.08 mag to the right. For comparison, the solid blue line represents the cross-SGB profile of a single-SSP simulation of NGC 1651, divided by a factor of $\simeq 3.5$ in order to scale its maximum density to that of NGC 1651. *Panel (b)*: Comparison between "multi-SSP" simulations of NGC 1651 created with binary fractions 0.0 (long dashed line), 0.2 (solid line), and 0.4 (short dashed line).

a distribution of ages similar to that implied by its cross-MSTO profile, rather than by a single SSP. This conclusion is opposite to that of L+14, who stated that the cross-SGB profile of NGC 1651 "can be explained only by a single-age stellar population, even though the cluster has a clearly extended main-sequence turn-off region" (quoting their abstract). Since both conclusions were drawn from the same original dataset, we discuss this disagreement in some detail below.

The analysis methods of L+14 differ in two main ways from those of ours. One difference is that L+14 did not use SSP simulations in their analysis. The ages in their cross-SGB profiles (their Fig. 4) were determined directly from the location of the isochrones in the CMD, thus only involving single stars. Conversely, we use SSP simulations including measurement errors and unresolved binary stars in this context. We note that the binary fractions of intermediate-age star clusters like NGC 1651 are substantial ($\approx$20%, Mackey et al. 2008; Milone et al. 2009; G+11a; G+14), and our simulations show that binaries extend the luminosity distribution of the SGB towards brighter magnitudes at the ages of such clusters (see, e.g., Fig. 2b). The effect of the binary fraction on the cross-SGB profile shape is illustrated in Fig. 3b for binary fractions of 0%, 20%, and 40%. Secondly and perhaps more importantly, L+14 did not take the stars in the SGB region of the CMD located above their log [age (yr)] = 9.24 isochrone into account (see their Figs. 2 and 4). Given our results shown in Fig. 3a, we suspect that if they would have done so, they would have found that the cross-SGB profile of NGC 1651 continues up to brighter magnitudes (equivalent to younger ages) with a profile shape that is clearly wider than that of a single SSP.

Finally, the *offset* in magnitude between the cross-SGB profile of NGC 1651 and that of its SSP simulations is also likely relevant to the disagreement between the conclusions of L+14 and ours, since L+14 based their conclusions in part on the observation that the age distribution measured from the cross-SGB profile of NGC 1651 reached an age lower than that measured from its cross-MSTO profile (cf. their Fig. 4). This will be discussed below.

3.2.2 *IC 2146*

We recall that this cluster was included in our sample because its mass and age are similar to those of NGC 1651; while NGC 1651 features an eMSTO, IC 2146 does not[3]. As such it provides a relevant comparison in the context of the nature of the SGB morphologies of such clusters.

Figure 4b shows a comparison between the cross-SGB profiles of IC 2146 (black line) and that of its single-SSP simulation (blue solid line). Note that in this case, the width of the profile of the single-SSP simulation is very similar to that of the cluster itself. This difference with respect to NGC 1651 is consistent with IC 2146 not hosting an eMSTO whereas NGC 1651 does, although this may in principle also be due in part to the larger photometric errors in the dataset of IC 2146 relative to those of the other clusters presented in this paper. However, an important result of the simulations of IC 2146 is that *the magnitude offset between the cross-SGB profiles of NGC 1651 and its SSP simulation (cf. above) is also present for IC 2146*. This suggests that the cause of this offset is *not* related to the question whether or not an intermediate-age cluster hosts an eMSTO (or a distribution of stellar ages). Instead, we suggest that the offset is of a systematic nature, related to one or more parameters relevant to the MSTO-SGB era of stellar evolution theory for stars of moderate metallicity and masses of ≈ 1.5 $M_{\odot}$. This is explored further in Sect. 4.

3.2.3 *NGC 1783, NGC 1806, and NGC 1846*

We performed a similar analysis of the SGB regions in the massive eMSTO clusters NGC 1783, NGC 1806, and NGC 1846, using the data from Goudfrooij et al. (2009) and G+11a. Since the ages of these three clusters are very similar to one another, we adopt the M+08 isochrone for an age of 1.65 Gyr to set the magnitude zeropoint for the cross-SGB profiles of these clusters. The results are shown in Figs. 5 – 7. Similar to the case of NGC 1651, we find that the shapes of the cross-SGB profiles of all three clusters are consistent with those of their respective multi-SSP simulations, while they are significantly wider than those of their single-SSP simulations. And again, the clusters' cross-SGB profiles are offset

[3] G+14 suggested that this difference is due to their different escape velocities.

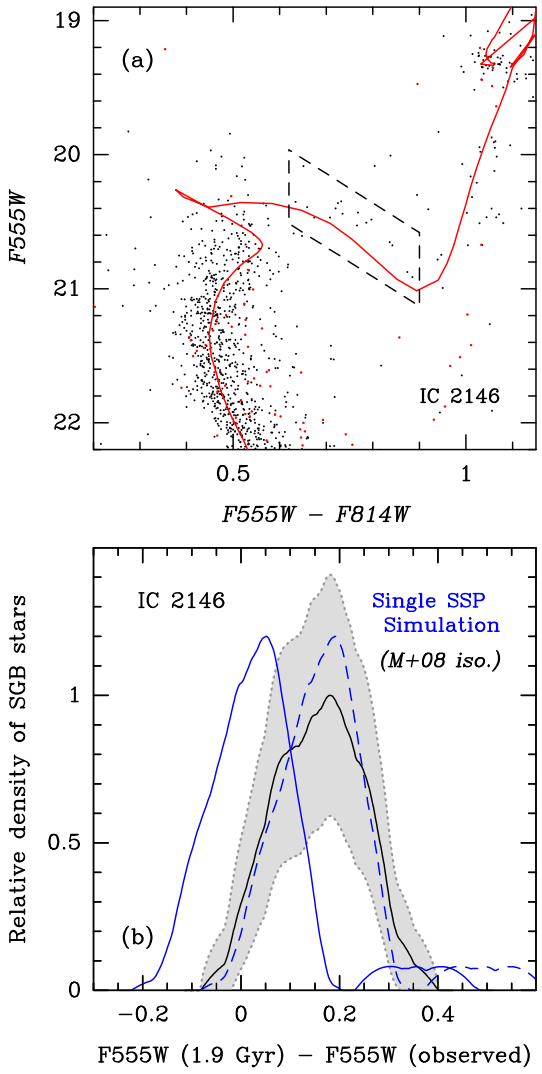

Figure 4. *Panel (a)*: CMD of IC 2146 within its core radius, taken from Correnti et al. (2014), along with a M+08 isochrone of age 1.90 Gyr. The SGB selection box is outlined by black dashed lines. Red dots indicate stars in the outskirts of the *HST* image with a total area equal to that within the core radius of IC 2146. *Panel (b)*: The black solid line represents the cross-SGB profile for IC 2146, while the light grey region indicates its 68% confidence interval. For comparison, the solid blue line represents the cross-SGB profile of a single-SSP simulation of IC 2146. The blue dashed line is the same after shifting it by 0.13 mag to the right.

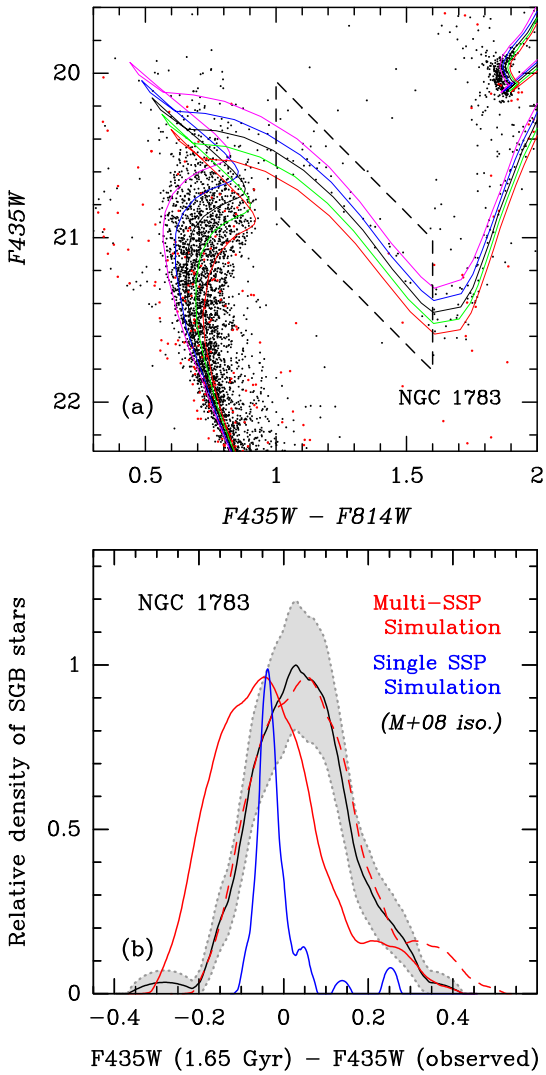

Figure 5. *Panel (a)*: CMD of NGC 1783 within its core radius, taken from G+11a, along with M+08 isochrones of age 1.50, 1.60, 1.70, 1.80, and 1.90 Gyr (top to bottom). Red dots indicate stars in the outskirts of the *HST* image with a total area equal to that within the core radius of NGC 1783. The SGB selection box is outlined by black dashed lines. *Panel (b)*: Similar to Figure 3, but now for NGC 1783. The SGB profile of the "Single SSP Simulation" was divided by a factor of $\simeq 4.5$ in order to scale its maximum density to that of NGC 1783.

from those of their multi-SSP simulations by a shift of $\simeq 0.08$ mag. Similar to the interpretation of this offset by L+14 for the case of NGC 1651, BN15 interpreted this offset for the cases of NGC 1806 and NGC 1846 in the sense that their SGB morphologies are inconsistent with the presence of a significant age spread[4].

[4] Note however that the *shapes* of the SGB profiles of NGC 1806 and NGC 1846 shown by BN15 (see their Figs. 3 and 8) seem to be more consistent with their SSP simulations that involve a spread of ages than with those of a single-age SSP.

3.2.4 *Summary*

Summarizing the results in this Section, it seems that the *shapes* of cross-SGB profiles of eMSTO clusters are consistent with those of their respective multi-SSP simulations, while they are inconsistent with those of their single-SSP simulations. Note that in this sense, the cross-SGB profiles of such clusters are entirely consistent with their cross-MSTO profiles when the latter are interpreted as a distribution of ages (i.e., the pseudo-age distributions derived by G+11a and G14).

The main inconsistency between the cross-SGB profiles of eMSTO clusters and those of their respective multi-SSP simulations shown above is that of an magnitude offset of ≈ 0.1 mag between them (for the filters of the *HST* instruments used here, i.e., F475W of WFC3 and F435W and F555W of ACS/WFC) in that the clusters' SGB stars are brighter than the simulations that use

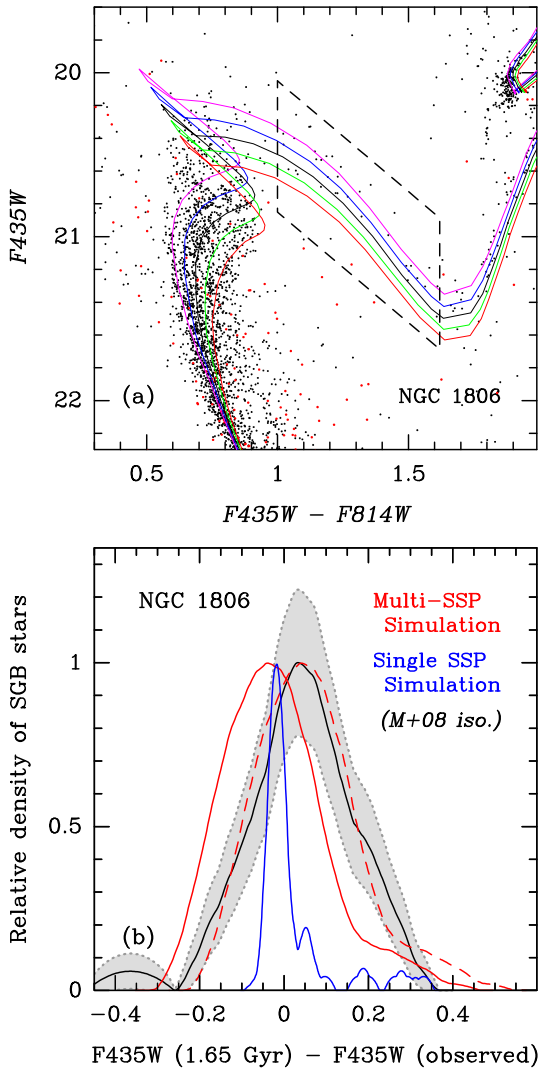

Figure 6. Similar to Figure 5, but now for NGC 1806. The SGB profile of the "Single SSP Simulation" in panel (b) was divided by a factor of $\simeq 4.6$ in order to scale its maximum density to that of NGC 1806.

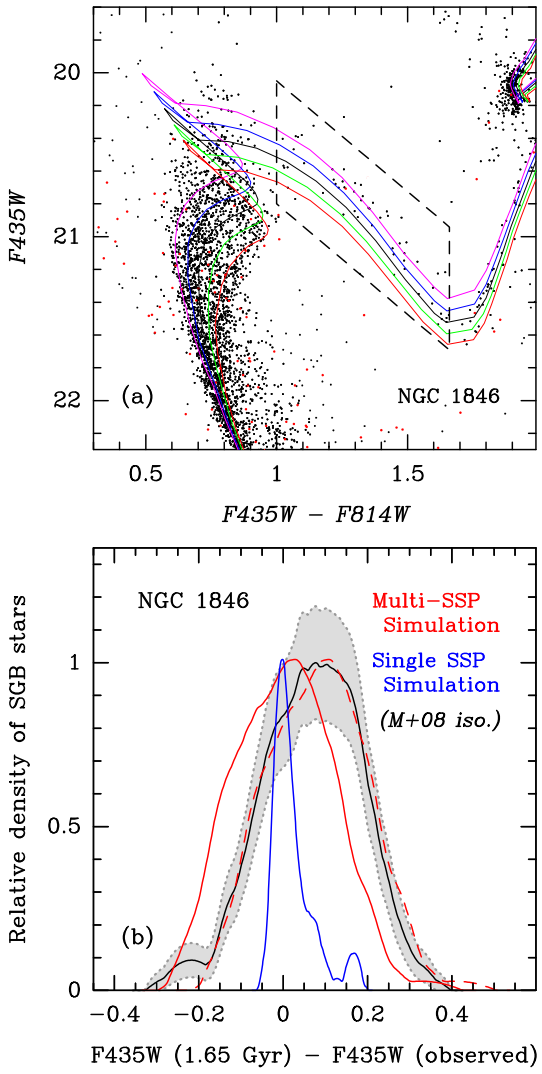

Figure 7. Similar to Figure 5, but now for NGC 1846. The SGB profile of the "Single SSP Simulation" in panel (b) was divided by a factor of $\simeq 4.4$ in order to scale its maximum density to that of NGC 1846.

their best-fitting M+08 isochrones. This issue is addressed in the next Section.

4 DISCUSSION

4.1 The Impact of Convective Overshoot

Stars in the MSTO and SGB region of the CMD for ages of $\sim 1.5-2.5$ Gyr have masses in the range $1.3 \lesssim (\mathcal{M}/M_{\odot}) \lesssim 1.6$. One parameter in stellar evolution theory that is known to have a significant impact on the photometric properties of stars in this mass range is that of the level of "overshoot" from the convective core, i.e., the mean free path of convective bubbles across the border of the convective region (e.g., Meader 1975; Bressan, Chiosi, & Bertelli 1981; Bertelli, Bressan, & Chiosi 1985; Demarque et al. 2004). The level of convective overshoot Λ_c depends on stellar mass in the mass range between fully radiative cores ($\mathcal{M} \lesssim 1.0\ M_{\odot}$) and that of fully convective cores ($\mathcal{M} \gtrsim 1.5\ M_{\odot}$), and it is also believed to depend on metallicity (Demarque et al. 2004; Bressan et al. 2012). The detailed dependencies of Λ_c on stellar mass and metallicity are not well-established, due in part to a relative lack of high-quality data of massive intermediate-age star clusters for calibration purposes. A consequence of this uncertainty is that different SSP models implement the dependencies of Λ_c on stellar mass and metallicity in different ways (compare, e.g., Pietrinferni et al. 2004; Dotter et al. 2008; Marigo et al. 2008; Bressan et al. 2012).

In the following we investigate whether an adjustment of the level of overshoot can reasonably account for the observed magnitude offset between the SGB profiles of clusters and those of their SSP simulations. To do so, we run a set of isochrones based on PARSEC tracks (Bressan et al. 2012) using a range of Λ_c. The model set covers $0.30 \leq \Lambda_c \leq 0.70$, where values for Λ_c are in the Bressan et al. (1981) formalism[5], for a range of ages and metallicities relevant to the clusters presented in this paper. Note that there are additional ways to adjust the level of overshooting for a given isochrone, such as shifting the stellar mass range in which over-

[5] Λ_c refers to the maximum level of overshoot in the relevant stellar mass range. The increase of overshoot level with stellar mass is assumed to be linear.

shooting takes place or by adopting a diffusive approach for this process (e.g., Freytag et al. 1996; Herwig 2000).

Fig. 8a shows the CMD of NGC 1651 along with three PARSEC isochrones with levels of overshoot ranging from $\Lambda_c = 0.35$ to 0.50. For each case, the age of the isochrone was adjusted to coincide with the best-fitting isochrone from the M+08 models (shown in Fig. 2, and with a black solid line in Fig. 8) near the red end of the turnoff region (at F475W $\simeq$ 21.15 and F475W−F814W $\simeq$ 0.82 to be precise). The values for $(m-M)_0$ and A_V were chosen to reproduce the positions of the RGB, the lower MS, and the red clump (RC), in a way equivalent to that described by G+11a. Note that the shape and location of the top of the MSTO of the PARSEC isochrone with $\Lambda_c = 0.40$ are virtually identical to those of the best-fitting M+08 isochrone, *while its SGB is clearly brighter* (by up to $\sim$0.12 mag at the red end of the SGB). Apart from this difference at the SGB and a small colour difference at the bottom of the MSTO, the PARSEC isochrone with $\Lambda_c = 0.40$ provides a fit to the CMD features of NGC 1651 that is very similar to that of the best-fitting M+08 isochrone. Fig. 8b illustrates the impact of the use of this PARSEC isochrone with $\Lambda_c = 0.40$ for creating cross-SGB profiles of NGC 1651 and its SSP simulations. This plot represents a copy of Fig. 3 except that the zeropoint of the SGB magnitude offsets is now set by the PARSEC isochrone rather than the best-fitting M+08 isochrone. *Note that the cross-SGB profile of NGC 1651 is now fully consistent with that of its multi-SSP simulation* (i.e., without any residual shift), *while its single-SSP simulation is still clearly narrower*.

Given this result, we suggest that the observed magnitude offsets between the SGB profiles of star clusters and those of their SSP model isochrones or simulations can be understood entirely by details of the way the dependencies of Λ_c on stellar mass and metallicity are implemented in the SSP model being used. As such, we argue against the use of the presence of such (small) magnitude offsets between cross-SGB profiles to confirm or deny the presence of a given age distribution in intermediate-age star clusters such as the ones discussed in L+14, BN15, and the current paper. Instead, we suggest that comparisons between SGB properties of such clusters and their SSP model predictions be focused on the *shapes* of their cross-SGB profiles, for clusters with statistically sufficient numbers of stars on the SGB, and that unresolved binaries are properly taken into account in such analyses.

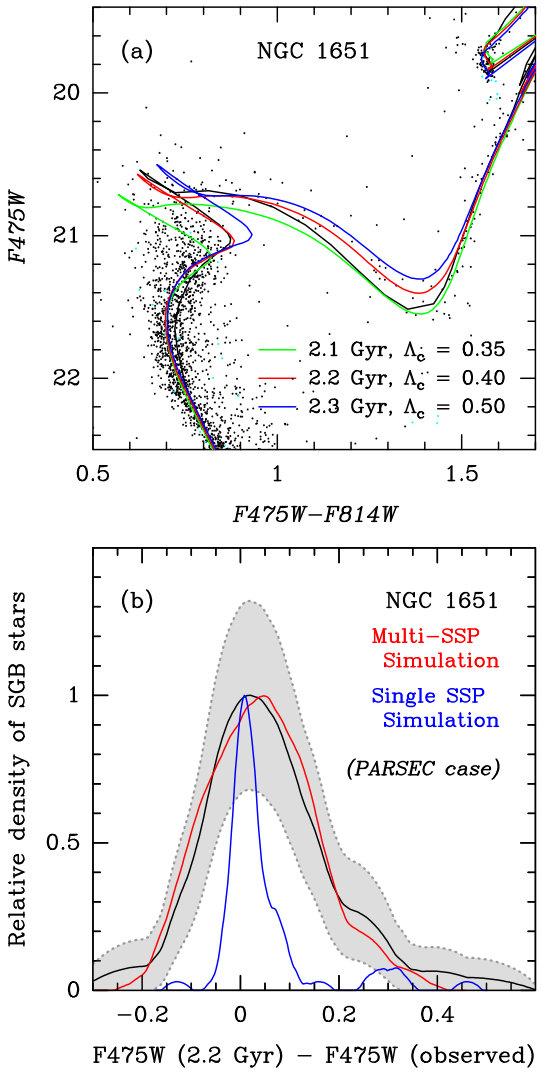

Figure 8. *Panel (a)*: CMD of NGC 1651 showing the upper MS, MSTO, SGB, lower RGB, and Red Clump features. The black line represents the best-fitting Marigo et al. (2008) isochrone (cf. Fig. 2a). The green, red, and blue lines represent PARSEC isochrones with [M/H] = –0.40 for which the ages and overshoot values are indicated in the legend. *Panel (b)*: Same as Fig. 3, but now using the SGB of the PARSEC isochrone with age = 2.2 Gyr and $\Lambda_c = 0.40$ as the zeropoint of the cross-SGB profiles. Note the similarity of the cross-SGB profiles of NGC 1651 (black line with 68% confidence interval in light grey) and that of its "multi-SSP simulation" (red line), while the cross-SGB profile of the "single-SSP simulation" (blue line) is much narrower.

4.2 The width of the Red Clump as a diagnostic for age spreads

In addition to their study of the shapes of the SGB, BN15 also presented a comparison between the RCs in NGC 1806 and NGC 1846 and those of M+08 isochrones of different ages (their Figs. 4 and 9), concluding (1) that the observed RC's showed a smaller spread in colour than expected from clusters having a significant age spread, and (2) that the isochrones that fit the youngest part of the eMSTO were also those that showed the best fit to the mean RC position.

To put BN15's analysis in context, we call attention to a few points that are relevant to the interpretation of the RC's position and width. First, the (mean) position of the RC depends on a number of factors in addition to age, distance, and reddening. One such factor is the mixing-length parameter $\alpha_{\rm MLT}$, which defines the efficiency of energy transport in the external layers of the star and hence its effective temperature $T_{\rm eff}$ for a given luminosity. In most isochrone sets, including the M+08 ones, $\alpha_{\rm MLT}$ is calibrated in the solar model, and then applied to all stars including the red giants. Recent 3-D model atmospheres from Trampedach et al. (2014) indicate however that while the approximation of a nearly constant $\alpha_{\rm MLT}$ might be good for stars along the upper RGB (and probably also for the RC), it also indicates significant variations between the $\alpha_{\rm MLT}$ values of red giants and those of dwarfs such as those populating the MS of Magellanic Cloud clusters. The variations are such (a few tenths in $\alpha_{\rm MLT}$) that they could change the relative colours of MS and RC stars by a few hundredths of a mag. Another uncertainty in isochrone colours is due to the adopted $T_{\rm eff}-$colour relations, which are usually derived from 1-D static model atmospheres (e.g., Castelli & Kurucz 2003). Therefore, one should be cautious in interpreting issues with regard to ages of star clusters based on differences between the MS and RC positions in the CMD, relative to isochrones, at levels of 0.01 – 0.03 mag.

As to the width of the observed RC, we agree with BN15 that it is compact in both NGC 1806 and NGC 1846, with its main component spanning just ≈ 0.5 mag in F435W – F814W colour. However, both NGC 1806 and NGC 1846 also exhibit a number of secondary RC stars (hereafter SRC; Girardi et al. 2009; G+14). These are He-burning stars that were massive enough to avoid electron degeneracy settling in their cores after leaving the main sequence. In both clusters, the SRC stars define an almost vertical feature to the bottom left of the main RC, centered at F435W – F814W $\simeq 1.80$ mag, and with F814W magnitudes between 18.4 and 18.7 (see Fig. 9); they are seen also in BN15's plots and are somewhat better delineated in NGC 1806 than in NGC 1846. These SRC sequences are, by themselves, a clear indication that *the RC in these clusters is not as homogeneous and compact* as claimed by BN15. In the age-spread interpretation of eMSTOs, the presence of a SRC is simply reflecting the spread in ages (i.e., initial stellar masses) of stars leaving the MSTO, and indeed the fraction of RC stars in the SRC among eMSTO clusters correlates strongly with the fraction of MSTO stars at the youngest (brightest) end of the MSTO (G+14). In the rotating scenario, instead, SRC stars are the putative progeny of fast MS rotators, since rapidly rotating stars have larger core masses at the end of the MS era than do nonrotating stars (e.g., Maeder & Meynet 2000; Eggenberger et al. 2010). However, this does not seem to explain the aforementioned observed correlation with the brighter part of the eMSTO (see G+14 for more details).

That said, it is interesting to note that such SRCs in NGC 1806 and NGC 1846 apparently contrast with comparatively narrow "main" RCs. As noticed by BN15, M+08 isochrones of ages between 1.3 and 1.8 Gyr span a significant range of RC colours (Δ(F435W – F814W) $\simeq 0.1$ mag), which seems wider than the RC colour spreads in their Figs. 5 and 10. There are however two additional points to be taken in consideration in this context: firstly, BN15 inferred the age distribution from the stars in the RC by assigning ages based on the "closest isochrone" rather than using a smooth function. This method introduces an intrinsic binning in the age distribution, with a bin size depending on the age spacing of the isochrones. Secondly, the M+08 isochrones were created by the interpolation of evolutionary tracks (originally taken from Girardi et al. 2000) which, for the mass interval into consideration ($\mathcal{M} \simeq 1.5 - 1.8\ M_\odot$), were computed for initial masses spaced by $\Delta\mathcal{M} = 0.05\ M_\odot$. The issue with such isochrones in the context of the interpretation of the RC morphologies of these star clusters is that they cannot reveal any CMD structure caused by variations in stellar evolutionary behaviour that occur over a mass interval smaller than $0.05\ M_\odot$. If any such variations occur, the isochrones' behaviour as a function of age will reflect the *smooth interpolation* between the confining tracks, rather than the real expected behaviour. This is what we believe is happening with the M+08 isochrones.

As recently noticed by Girardi et al. (2013b, see their appendix), the onset of electron degeneracy in stellar cores at $\mathcal{M} \lesssim 1.7\ M_\odot$ (with the exact limiting value depending on overshooting efficiency) produces a marked discontinuity in the evolutionary behaviour of stars, occurring over a mass scale smaller than $0.01\ M_\odot$. This significantly affects the expected shape of the RC in more detailed isochrone models, where stars are in principle expected to be either on the main RC or in the SRC, but rarely in between these features (modulo unresolved binary stars). As a consequence, the RC is expected to be more compact than that displayed in M+08 isochrones. The expectation from PARSEC isochrone models computed from tracks with a fine grid of stellar masses – namely those derived from a $Z = 0.008$ grid with the same level of detail and mass resolution as in Girardi et al. (2013b, i.e., $\Delta\mathcal{M}/M_\odot = 0.01$) – is shown in Fig. 9a, and compared with M+08 isochrones (Fig. 9b) using the same values for $(m-M)_0$ and A_V. In both cases, we superimpose the stars observed within the core radius of NGC 1806. It can be seen that, with the new PARSEC models, the extent of the observed "main" RC appears to be compatible with an age range of $\Delta\log(\text{age}) \simeq 0.10$ (or $\Delta(\text{age}) \simeq 500$ Myr at an average age of 1.7 Gyr), whereas it indicates a smaller age range in the case of the M+08 isochrones ($\Delta\log(\text{age}) \simeq 0.07$ or $\Delta(\text{age}) \simeq 200$ Myr).

The ability of the new PARSEC isochrone models that were computed from a grid of initial stellar masses spaced by $\Delta\mathcal{M} = 0.01\ M_\odot$ to fit the full CMD of NGC 1806 is illustrated in Fig. 9c. We used $(m-M)_0 = 18.53$ mag and $A_V = 0.035$ mag for these isochrones. Note the good fit to the MSTO, SGB, RGB, and RC regions.

Finally, we determine the age distribution from the RC of NGC 1806 by means of the distribution of stars in a rectangle in the RC region of the F814W vs. F435W – F814W CMD. The short and long axes of the rectangle are approximately parallel and perpendicular to the isochrones, respectively (see blue rectangle in Fig. 9b). The magnitudes and colours of stars in the rectangle are then transformed into the coordinate frame defined by its two axes. The star positions in the coordinate perpendicular to the isochrones are then translated to age by repeating the same procedure for the new PARSEC isochrone tables described above, for an age range that fully covers the observed extent of the RC region of NGC 1806 (using the same values of Z, $(m-M)_0$ and A_V), and performing a polynomial least-squares fit between age and the coordinate perpendicular to the isochrones[6]. The resulting age distribution of NGC 1806 is shown in Fig. 9d (black line), using a non-parametric Epanechnikov density kernel as before. For comparison, Fig. 9d also shows the age distribution that would be expected for a single SSP, derived from a set of Monte Carlo simulations (as described in Sect. 3.1) using the new PARSEC isochrone for an age of 1.74 Gyr. Note that while the age distribution is shifted to slightly older ages relative to those indicated by the cross-MSTO profiles when the latter are compared with M+08 isochrones (cf. Fig. 1c), the cross-RC profile shape of NGC 1806 is similar to that of its cross-MSTO one, and it is significantly wider than that of a single-SSP simulation.

Although these new RC models will be described in more detail in a forthcoming paper, these results already demonstrate that the expected detailed RC morphology of intermediate-age clusters that host a range of stellar ages is model –and mass-resolution– dependent. We therefore argue that the conclusions by BN15 on the nature of the RCs of NGC 1806 and NGC 1846 were largely due to their choice of isochrones and analysis methods. In contrast, our results with newly updated isochrone models strongly suggest that the RC morphologies of these clusters are actually *described very well by a distribution of stellar ages that is consistent with that indicated by their MSTOs*.

4.3 Implications regarding the nature of eMSTOs

Our result that the widths and shapes of cross-SGB profiles of eMSTO clusters are consistent with those of their respective multi-SSP

[6] We excluded the SRC area of the CMD from this rectangle to avoid the highly non-linear (and multi-valued) functional relation between age and the coordinate along the long axis of such a rectangle in the SRC region. This causes an underestimate of the number of stars at the youngest ages shown in Fig. 9d.

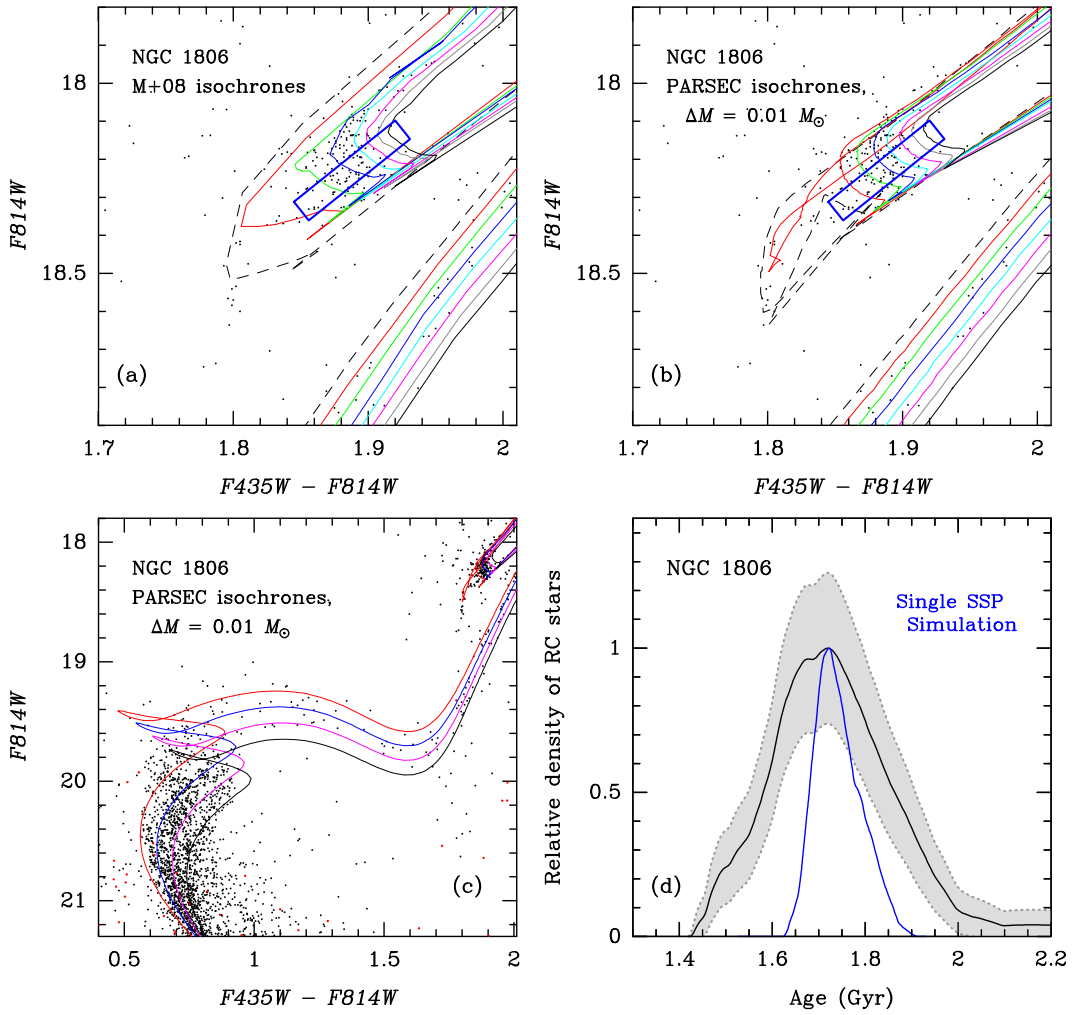

Figure 9. *Panel (a)*: The CMD of NGC 1806 (cf. Fig. 6a), zoomed in on the RC region. The lines represent Marigo et al. (2008) isochrones for log (age/yr) = 9.10 to 9.24 (left to right) with a spacing of 0.02. *Panel (b)*: Same as panel (a), but the lines now represent new PARSEC isochrones with $Z = 0.008$ which were derived from stellar tracks spaced by $\Delta\mathcal{M}/M_{\odot} = 0.01$ (see Sect. 4.2). Isochrones are for log (age/yr) = 9.18 to 9.32 (left to right) with a spacing of 0.02. The thick blue rectangle in panels (a) and (b) is used to derive the age distribution of RC stars as described in Sect. 4.2. *Panel (c)*: CMD of NGC 1806 showing the region from below the MSTO to beyond the RC along with new PARSEC isochrones for $Z = 0.008$ and ages of 1.58, 1.74, 1.91, and 2.09 Gyr (left to right). *Panel (d)*: The black solid line shows the cross-RC distribution of NGC 1806 expressed in age units (see Sect. 4.2), while the light grey region indicates its 68% confidence interval. For comparison, the solid blue line represents the cross-RC distribution of a single-SSP simulation of NGC 1806, divided by a factor $\simeq 1.9$ to yield the same maximum star density as that of NGC 1806 itself.

simulations, and significantly wider than those of their single-SSP simulations, has a number of interesting implications related to the nature of eMSTOs.

It is obvious that this result is consistent with the prediction of the "extended star formation" scenario; we therefore focus on a comparison with predictions of the "stellar rotation" scenario. It is well known that the centrifugal force in rotating stars with masses in the approximate range of $1.2-1.7\ M_{\odot}$ decreases their effective gravity which in turn lowers their effective temperature (e.g., Meynet & Maeder 1997). This prompted Bastian & de Mink (2009) to suggest that a range of stellar rotation velocities may cause the eMSTO feature. However, Girardi et al. (2011) computed an isochrone for a typical age of eMSTO clusters and a typical stellar rotation velocity and found that the prolonged lifetime of rotating stars approximately cancels the effects of the lower gravity in terms of the MSTO colour, which was found to be virtually equal to that of the non-rotating isochrone. The main impact of stellar rotation was found to be a *lengthening* of the MSTO hook in conjunction with a brightening of the SGB (see Fig. 3 in Girardi et al. 2011), similar to the effects of an increased level of convective overshoot shown in Sect. 4.1.

More recently, Yang et al. (2013) computed isochrones that included the effects of stellar rotation, using the Yale Rotating Evolution Code (Pinsonneault et al. 1989). They found that rotation can actually cause eMSTOs if the efficiency of rotational mixing is sufficiently small[7]. However, the luminosities of the onset of the SGB of the rotating isochrones was found to be consistent with those of the corresponding non-rotating isochrones. This was also part of the arguments of L+14, who used the recent tracks of Georgy et al.

[7] Note however that G+14 pointed out that the width of the MSTO of the most massive eMSTO clusters is significantly larger than the predictions of Yang et al. (2013), even for their smallest value of rotational mixing efficiency.

(2014) and showed that the track for a rapidly rotating star is at a cooler temperature than that of the non-rotating track at the MSTO, while the rotating track merges with the non-rotating track right at the onset of the SGB. However, we remind the reader that due to the longer lifetime of rotating stars, one should not use stellar tracks to interpret the morphologies of the MSTO or SGB in CMDs. One should compute isochrones instead. This will be addressed in a forthcoming paper.

In summary, a spread of rotational velocities in a single-age stellar population would cause the MSTO and SGB features to show the following properties according to the predictions of the recent modeling efforts:

- According to the findings of Girardi et al. (2011), the MSTO would not show any significant spread in colour, only a spread of the *length* of the MSTO hook. This is inconsistent with the MSTO morphologies of eMSTO clusters. Conversely, the SGB *would* show a significant spread of luminosities (similar to what we find in eMSTO clusters).
- According to Yang et al. (2013) and L+14, the MSTO would show some significant spread in colour (similar to the morphology of eMSTOs) if the efficiency of rotational mixing is small, but the luminosity of the SGB would *not* be affected in a significant way. The latter prediction is inconsistent with our cross-SGB profiles of eMSTO clusters.

Given the above, our result that the cross-SGB profiles of eMSTO clusters are significantly wider than that of their single-SSP simulations (and consistent with the widths of MSTOs of eMSTO clusters) seems to indicate that *their MSTO and SGB morphologies are better described by a distribution of stellar ages than by the combination of a single age and a range of stellar rotation velocities*. We recognize that the extent to which rapid stellar rotation affects the temperature and luminosity of SGB stars is still in some level of flux. For example, the grid of models by Georgy et al. (2014) has so far only been completed for stars with $\mathcal{M} \geq 1.7\,M_{\odot}$, while SGB stars in the eMSTO clusters discussed in this paper are less massive (by $0.1-0.3\,M_{\odot}$)[8]. As such, our conclusions refer to the situation at the time this paper is written.

5 SUMMARY AND CONCLUSIONS

In the context of the question of the nature of eMSTOs in massive intermediate-age star clusters in the LMC, we investigated the recent claims of Li et al. (2014, L+14) and Bastian & Niederhofer (2015, BN15) regarding the nature of such clusters' SGB morphologies, which are expected to be affected more by age spreads than by spreads in stellar rotation velocity. Their analysis led them to argue that the SGB morphologies of three clusters featuring eMSTOs (NGC 1651, NGC 1806, and NGC 1846) are inconsistent with extended star formation histories within those clusters. We performed an independent study of the SGB morphologies of five intermediate-age star clusters in the LMC, including the three clusters studied by L+14 and BN15 (NGC 1651, NGC 1806, and NGC 1846). Comparisons between the SGB morphologies of cluster stars and those of SSP model predictions are done using Monte-Carlo simulations of single-age SSPs as well as "composite SSPs" whose age distributions are taken from the "pseudo-age distributions" of the clusters which were derived from their MSTO morphologies by G+11a and G+14. The SSP simulations include a self-consistent treatment of unresolved binaries. Other methodological differences with the L+14 and BN15 studies are pointed out where relevant. Our main conclusions are the following.

(i) In contrast with L+14 and BN15, we find that the shapes of the cross-SGB profiles of all clusters in our sample are consistent with their cross-MSTO profiles (to within 1σ) when the latter are interpreted as distributions in age. Conversely, cross-SGB profiles of simulated single-age stellar populations (convolved with photometric uncertainties) are found to be significantly narrower than those of the clusters.

(ii) We argue that the magnitude offset between the cross-SGB distributions of the clusters in our sample and that of their best-fitting isochrones from the Marigo et al. (2008) family of SSP models can be understood once the variation of the treatment of convective overshoot among SSP isochrone models is taken into account.

(iii) We investigate the claims made by BN15 who stated that the red clumps of NGC 1806 and NGC 1846 showed a smaller spread in colour than expected from clusters having a significant age spread, and that the M+08 isochrones that fit the youngest part of the eMSTO were those that showed the best fit to the mean RC position. We find that these results are dependent on the models and methods used. Using isochrones newly created from a grid of PARSEC tracks that features a 5-fold higher resolution in stellar mass than that used by the M+08 (and most other sets of) isochrones, we find that ages indicated by the MSTO of NGC 1806 are actually *consistent* with those indicated by the RC. Furthermore, we find that the RC morphology of NGC 1806 is consistent with the age distribution indicated by the MSTO, and significantly more extended than that expected from a single-age SSP.

(iv) We compare the observed MSTO and SGB morphologies of eMSTO clusters with those of (current) predictions of models that assume (a) a distribution of stellar ages versus (b) a range of stellar rotation velocities at a single age. This comparison indicates that a distribution of stellar ages is currently the only option that can explain both the observed MSTO and SGB morphologies.

Our overall conclusion is that in spite of recent arguments by L+14 and BN15, the SGB and RC morphologies of star clusters featuring eMSTOs are consistent with the scenario in which eMSTOs are (mainly) due to a distribution of stellar ages.

Acknowledgments.
This work is based on observations obtained with the NASA/ESA *Hubble Space Telescope*, obtained at the Space Telescope Science Institute, which is operated by the Association of Universities for Research in Astronomy, Inc., under NASA contract NAS5-26555. Partial support for this project was provided by NASA through grant HST-GO-12908 from the Space Telescope Science Institute. We are grateful for a very thoughtful review by the anonymous referee, which improved this paper. P.M. and L.G. acknowledge support from the University of Padova (*Progetto di Ateneo 2012*, ID: CPDA125588/12), and from the ERC Consolidator Grant funding scheme (*project STARKEY*, G. A. n. 615604). T.H.P. acknowledges support through FONDECYT Regular Project Grant No. 1221005 and BASAL Center for Astrophysics and Associated Technologies (PFB-06). We acknowledge relevant discussions with Vera Kozhurina-Platais. We made significant use of the SAO/NASA Astrophysics Data System during this project, and we acknowledge use of the R Language for Statistical Computing, see http://www.R-project.org.

[8] We note that the study of Yang et al. (2013) showed that the impact of stellar rotation to isochrone shapes changes significantly in this mass range.

REFERENCES

Bastian N., de Mink S. E., 2009, MNRAS, 398, L11
Bastian N., Niederhofer F., 2015, MNRAS, in press (BN15; arXiv:1501.03835)
Bastian N., Silva-Villa E., 2013, MNRAS, 431, L122
Bastian N., Lamers H. J. G. L. M., de Mink S. E., Longmore S. N., Goodwin S. P., Gieles M. 2013, MNRAS, 436, 2398
Bedin L. R., Piotto G., Anderson J., Cassisi S., King I. R., Momany Y., ApJ, 605, L125
Bellini A., et al., 2013, ApJ, 765, 32
Bertelli G., Bressan A., Chiosi C., 1985, A&A, 150, 33
Bressan A., Chiosi C., Bertelli G., 1981, A&A, 102, 25
Bressan A., Marigo P., Girardi L., Salasnich B., Dal Cero C., Rubuel S., Nanni A., 2012, MNRAS, 427, 127
Carretta E., et al., 2010, A&A, 505, 117
Castelli F., Kurucz R. L., 2003, in IAU Symposium 210, Modeling of Stellar Atmospheres, N. Piskunov, W. W. Weiss, and D. F. Gray, eds, p. A20
Conroy C., Spergel D. N., 2011, ApJ, 726, 36
Correnti M., Goudfrooij P., Kalirai J. S., Girardi L., Puzia T. H. Kerber L., 2014, ApJ, 793, 121
Correnti M., Goudfrooij P., Puzia T. H., de Mink S. E., 2015, submitted to MNRAS
D'Antona F., Ventura P. 2007, MNRAS, 379, 1431
Decressin T., Meynet G., Charbonnel C., Prantzos N., Ekström S., 2007, A&A, 464, 1029
Demarque P., Woo J.-H., Kim Y.-C., Yi S. K., 2004, ApJS, 155, 667
D'Ercole A., Vesperini E., D'Antona F., McMillan S. L. W., Recchi S., 2008, MNRAS, 391, 825
Dotter A., Chaboyer B., Jevremović D., Kostov V., Baron E., Ferguson J. W., 2008, ApJS, 178, 89
Dotter A., Ferguson J. W., Conroy C., Milone A. P., Marino A. F., Young D., 2015, MNRAS, 446, 1641
de Mink S. E., Pols O. R., Langer N., Izzard R. G., 2009, A&A, 5007, L1
Eggenberger P., Miglio A., Montalban J., Moreira O., Noels A., Meynet G., Maeder A., 2010, A&A, 509, A72
Freytag B., Ludwig H.-G., Steffen M., 1996, A&A, 313, 497
Georgy C., Granada A., Ekström S., Meynet G., Anderson R. I., Wyttenbach A., Eggenberger P., Maeder A., 2014, A&A, 566, A21
Girardi L., Bressan A., Bertelli G., Chiosi C., 2000, A&AS, 141, 371
Girardi L., Rubele S., Kerber L., 2009, MNRAS, 394, L74
Girardi L., Eggenberger P., Miglio A., 2011, MNRAS, 412, L103
Girardi L., et al., 2013a, MNRAS, 431, 3501
Girardi L., Marigo P., Bressan A., Rosenfield P., 2013b, ApJ, 777, 142
Glatt K., et al., 2008, AJ, 135, 1703
Goudfrooij P., Puzia T. H., Kozhurina-Platais V., Chandar R., 2009, AJ, 137, 4988
Goudfrooij P., Puzia T. H., Kozhurina-Platais V., Chandar R., 2011a, ApJ, 737, 3 (G+11a)
Goudfrooij P., Puzia T. H., Chandar R., Kozhurina-Platais V., 2011b, ApJ, 737, 4 (G+11b)
Goudfrooij P., et al., 2014, ApJ, 797, 35 (G+14)
Gratton R., Carretta E., Bragaglia A., 2012, A&ARv, 20, 50
Herwig F., 2000, A&A, 360, 952
Li C., de Grijs R., Deng L., 2014, Nature, 516, 367 (L+14)
Li Z., Mao C., Chen L., Zhang Q., 2012, ApJ, 761, L22
Keller S. C., Mackey A. D., Da Costa G. S., 2011, ApJ, 731, 22
Keller S. C., Mackey A. D., Da Costa G. S., 2012, ApJ, 761, L5
Mackey A. D., Broby Nielsen P., 2007, MNRAS, 379, 151
Mackey A. D., Broby Nielsen P., Ferguson A. M. N., Richardson J. C., 2008, ApJ, 681, L17
Marigo P., Girardi L., Bressan A., Groenewegen M. A. T., Silva L., Granato G. L., 2008, A&A, 482, 883 (M+08)
Meader A., 1975, A&A, 40, 303
Maeder A., Meynet G., 2000, ARA&A, 38, 143
Meynet G., Meader A., 1975, A&A, 321, 456
Milone A. P., Bedin L. R., Piotto G., Anderson J., 2009, A&A, 497, 755
Milone A. P., et al., 2012, ApJ, 744, 58
Milone A. P., et al., 2013, ApJ, 767, 120
Milone A. P., et al., 2015, MNRAS, 447, 931
Pietrinferni A., Cassisi S., Salaris M., Castelli F., 2004, ApJ, 612, 168
Pinsonneault M. H., Kawaler S. D., Sofia S., Demarque P., 1989, ApJ, 338, 424
Piotto G., et al., 2007, ApJ, 661, L53
Piotto G., et al., 2012, ApJ, 760, 39
Rubele S., Girardi L., Kozhurina-Platais V., Goudfrooij P., Kerber L., 2011, MNRAS, 414, 2204
Rubele S., Girardi L., Kozhurina-Platais V., Kerber L., Goudfrooij P., Bressan A., Marigo P., 2013, MNRAS, 433, 2774
Rubele S., Kerber L., Girardi L., 2010, MNRAS, 403, 1156
Salpeter E. E., 1955, ApJ, 121, 161
Silverman B. W., 1986, in *Density Estimation for Statistics and Data Analysis*, Chap and Hall/CRC Press, Inc.
Trampedach R., Stein R. F., Christensen-Dalsgaard J., Nordlund Å, Asplund M., 2014, MNRAS, 445, 4366
Valcarce A. A. R., Catelan M., 2011, A&A, 533, A120
Yang W., Bi S., Meng X., Liu Z., 2013, ApJ, 776, 112

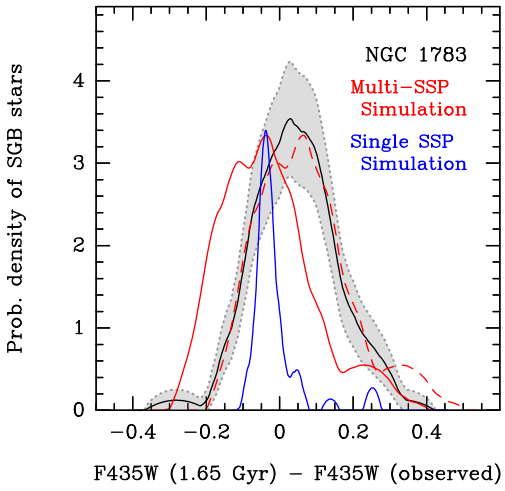
NGC 1783
Multi−SSP
Simulation
Single SSP
Simulation
Prob. density of SGB stars
0
1
2
3
4
−0.4
−0.2
0
0.2
0.4
F435W (1.65 Gyr) − F435W (observed)

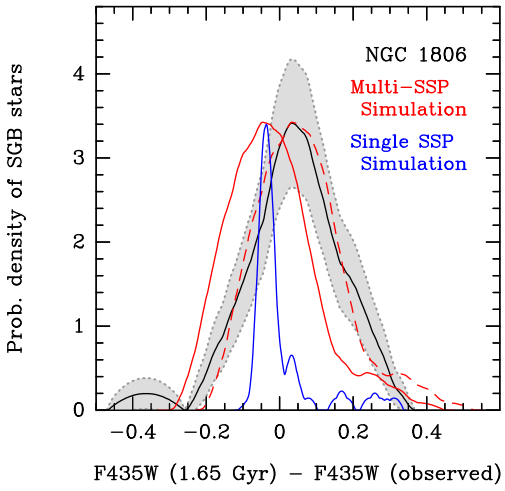
NGC 1806
Multi−SSP
Simulation
Single SSP
Simulation
Prob. density of SGB stars
F435W (1.65 Gyr) − F435W (observed)
0
1
2
3
4
−0.4
−0.2
0
0.2
0.4

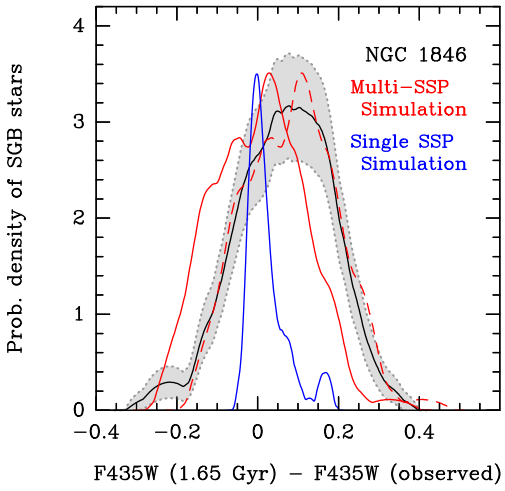
NGC 1846
Multi−SSP
Simulation
Single SSP
Simulation
Prob. density of SGB stars
F435W (1.65 Gyr) − F435W (observed)
0
1
2
3
4
−0.4
−0.2
0
0.2
0.4

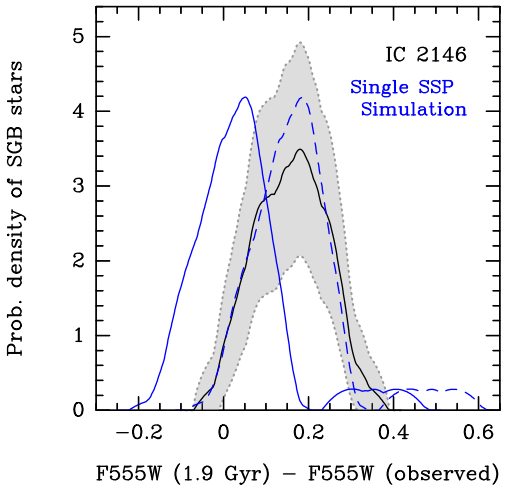
IC 2146
Single SSP
Simulation
Prob. density of SGB stars
F555W (1.9 Gyr) − F555W (observed)
0
1
2
3
4
5
−0.2
0
0.2
0.4
0.6